Supplementary Information

Assessing Energy Offset Between Electron Donor/acceptor Interface in Organic Solar Cells through Radiative Efficiency Measurement

Yuan Xie[a], Weiping Wang[b],Wei Huang[c], Fengyuan Lin[c], Tengfei Li[d], Sha Liu[a], Xiaowei Zhan[d], Yongye Liang*[c], Chao Gao*[b], Hongbin Wu*[a], Yong Cao[a]

[a]Institute of Polymer Optoelectronic Materials and Devices, State Key Laboratory of Luminescent Materials and Devices, South China University of Technology, Guangzhou, 510640, P. R. China.

[b] State Key Laboratory of Fluorine & Nitrogen Chemicals, Xi'an Modern Chemistry Research Institute, Xi'an, Shaanxi, 710065, P. R. China

[c]Department of Materials Science and Engineering, Shenzhen Key Laboratory of Printed Organic Electronics, South University of Science and Technology of China, Shenzhen 518055, P. R. China

[d]Department of Materials Science and Engineering, College of Engineering, Key Laboratory of Polymer Chemistry and Physics of Ministry of Education, Peking University, Beijing 100871, P. R. China

Corresponding Authors:

*E-mail: liangyy@sustech.edu.cn, chaogao1974@hotmail.com, hbwu@scut.edu.cn,

Supplementary Figures

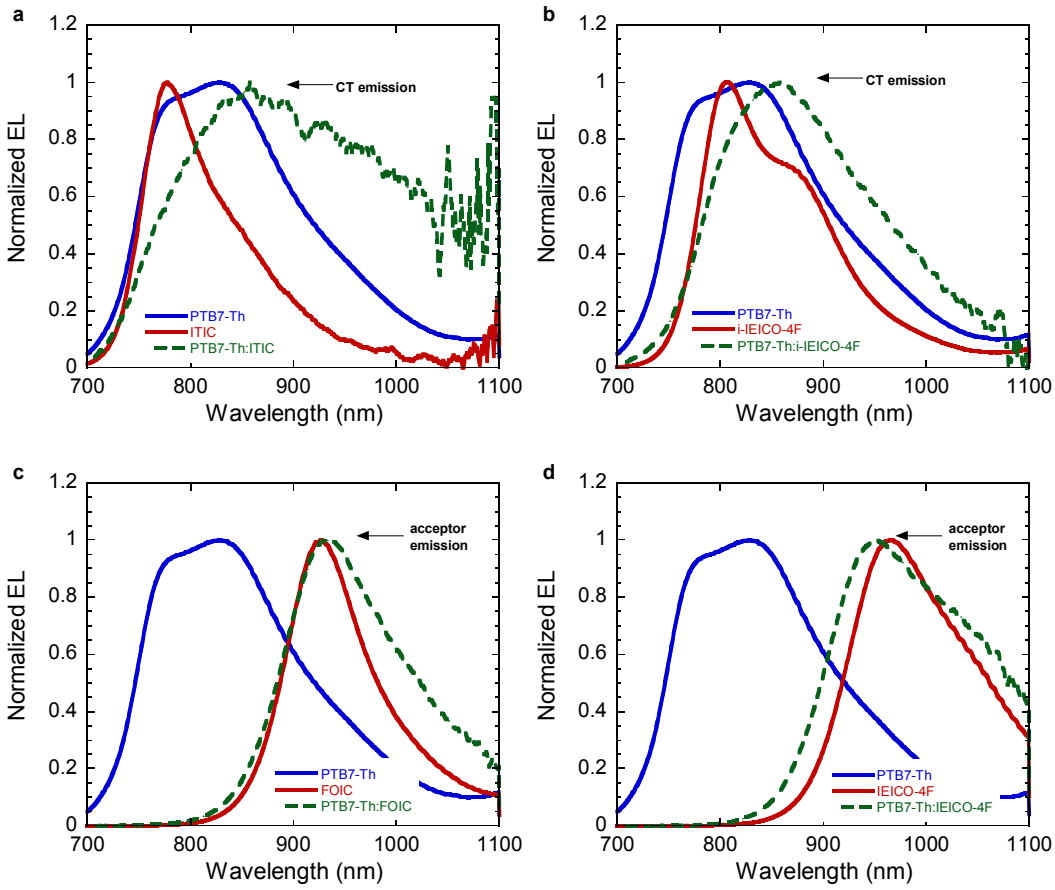

Supplementary Figure 1.Normalized EL spectra for PTB7-Th based devices. The EL spectra for PTB7-Th blending with acceptors with different HOMO levels. **a, b,** Blends with large HOMO offset manifest pronounced CT feature, where new emission peak shows up at lower energy region(long wavelength). **c, d**, In blends with small HOMO offset, the CT emission is vanishingly small so that the emission is dominated by the low bandgap acceptor.

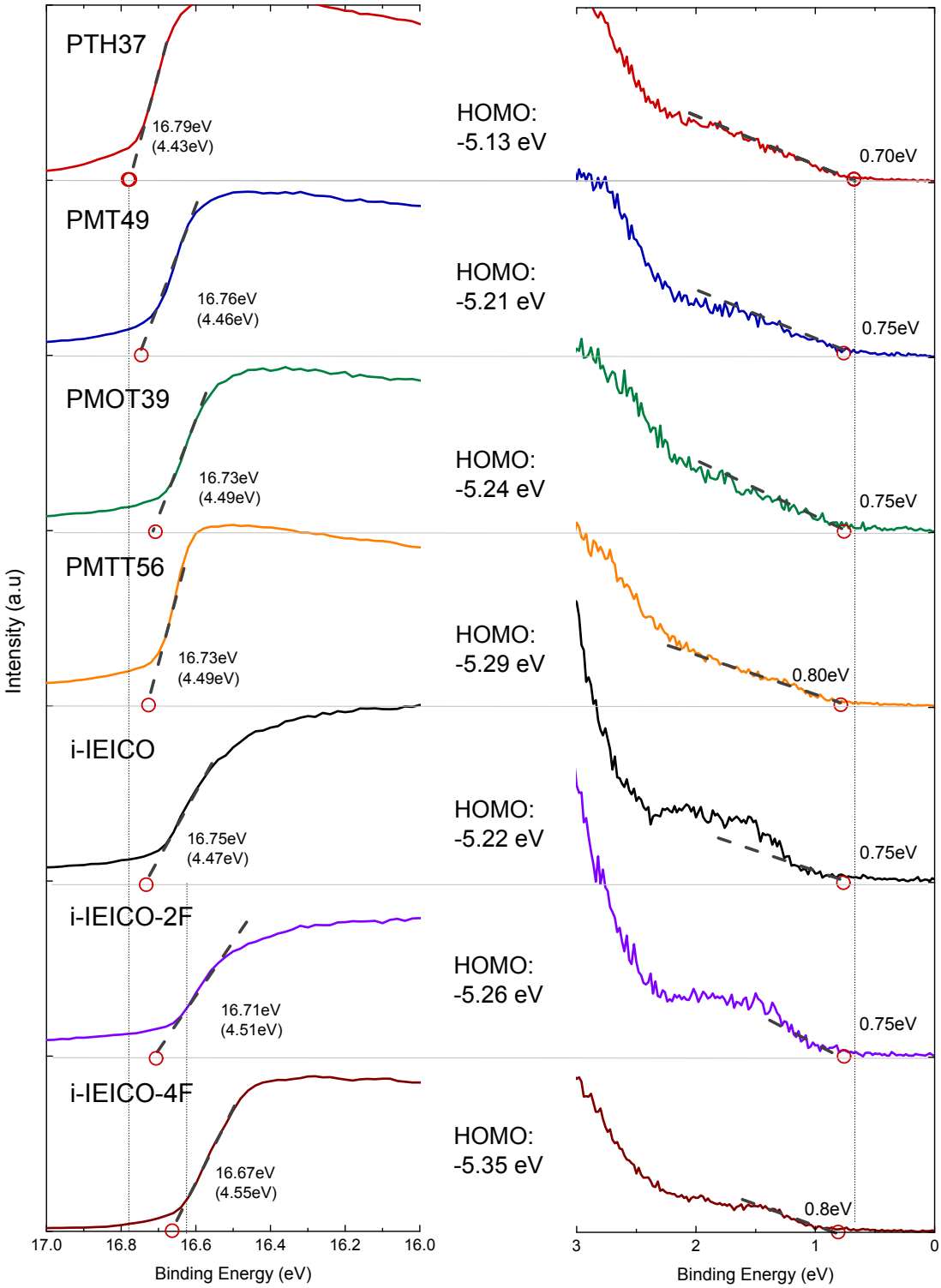

Supplementary Figure 2. Ultraviolet Photoelectron Spectroscopy (UPS) spectra. High binding energy cutoff(left) and HOMO region(right) of UPS spectra are shown for donors and acceptors. The spectra width is defined by energy difference between two regions, in which linear fit of slope intersects(grey dash line) with baseline gives the binding energy[1]. The

HOMO levels(middle) are calculated by subtracting the spectra width from the He I excitation energy (21.22 eV).

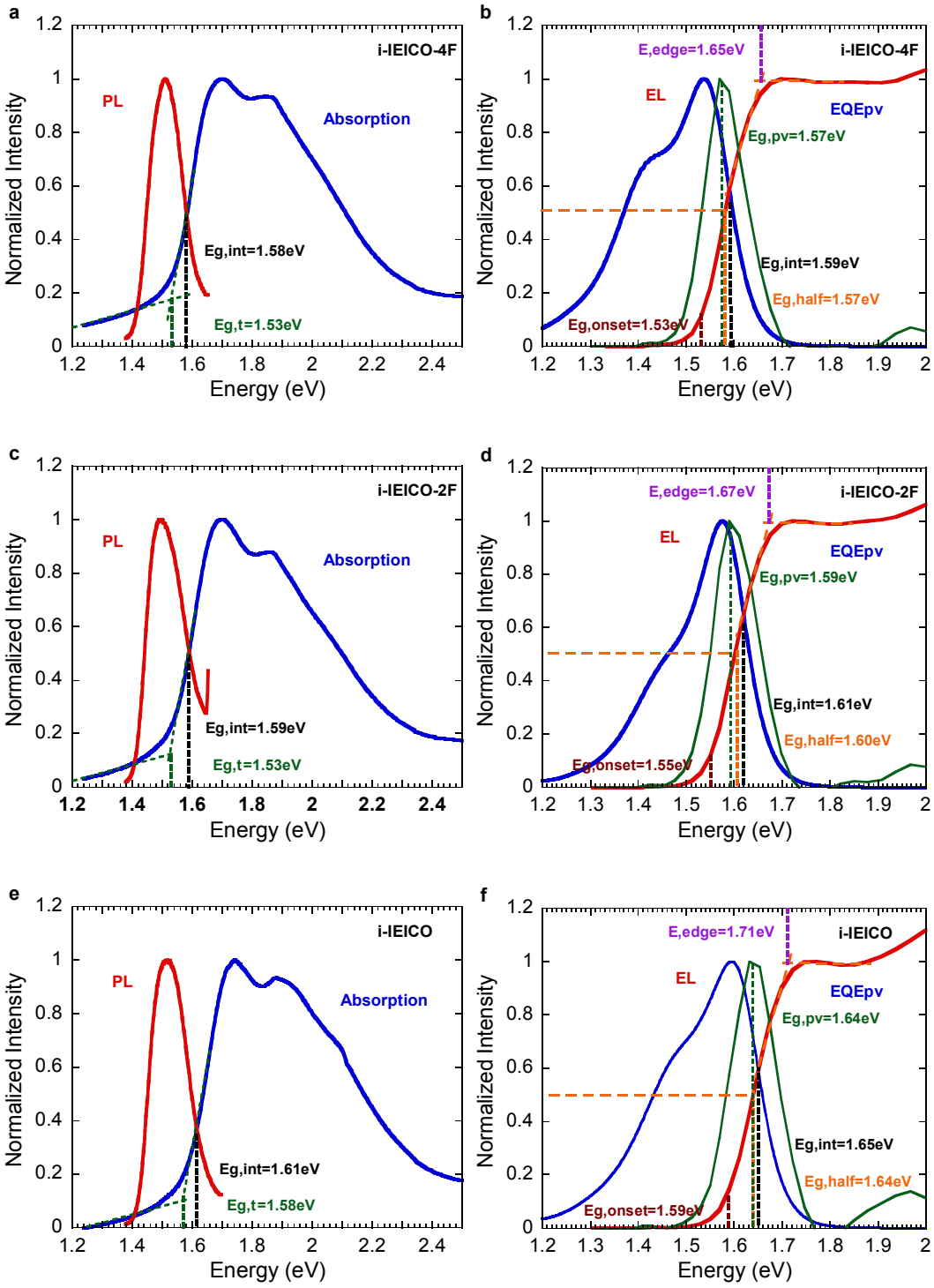

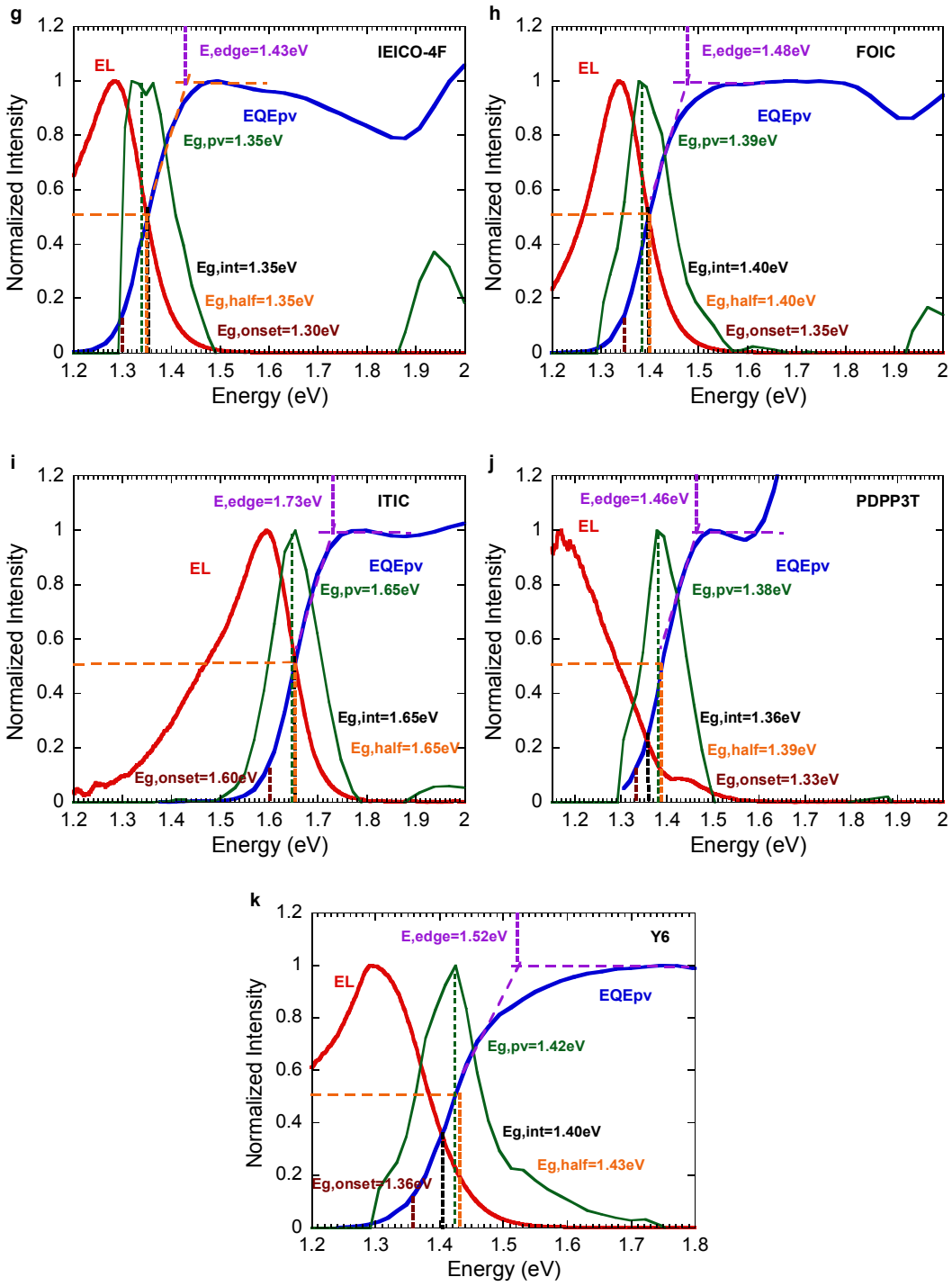

Supplementary Figure 3.Optical bandgap determined from different methods. The optical bandgap is determined by six different methods[2]. $E_{g,t}$ is the optical bandgap obtained by absorption onset and $E_{g,onset}$ is determined by the onset of external quantum efficiency (EQE_{PV}). E_{edge} denotes the optical bandgap that strongly absorb, is the energy intersection of extrapolated linear part of the absorption edge and low-energy peak of EQE_{PV}[3]. The energy intersection between normalized absorption and emission ($E_{g,int}$) offers a reliable method with

detailed photo-physical implication[4]. $E_{g,pv}$ is extracted from the maximum of the derivative of EQE_{PV}, representing an analogy to ideal Shockley-Queisser bandgap for real photovoltaic device[5].In this study, we use feasible $E_{g,half}$, the energy of half EQE_{PV} maximum from low bandgap absorbers, as optical bandgap to determine voltage loss. $E_{g,half}$ consistent well with both photo-physical and mathematical approach, providing nearly identical results as $E_{g,int}$ and $E_{g,pv}$.

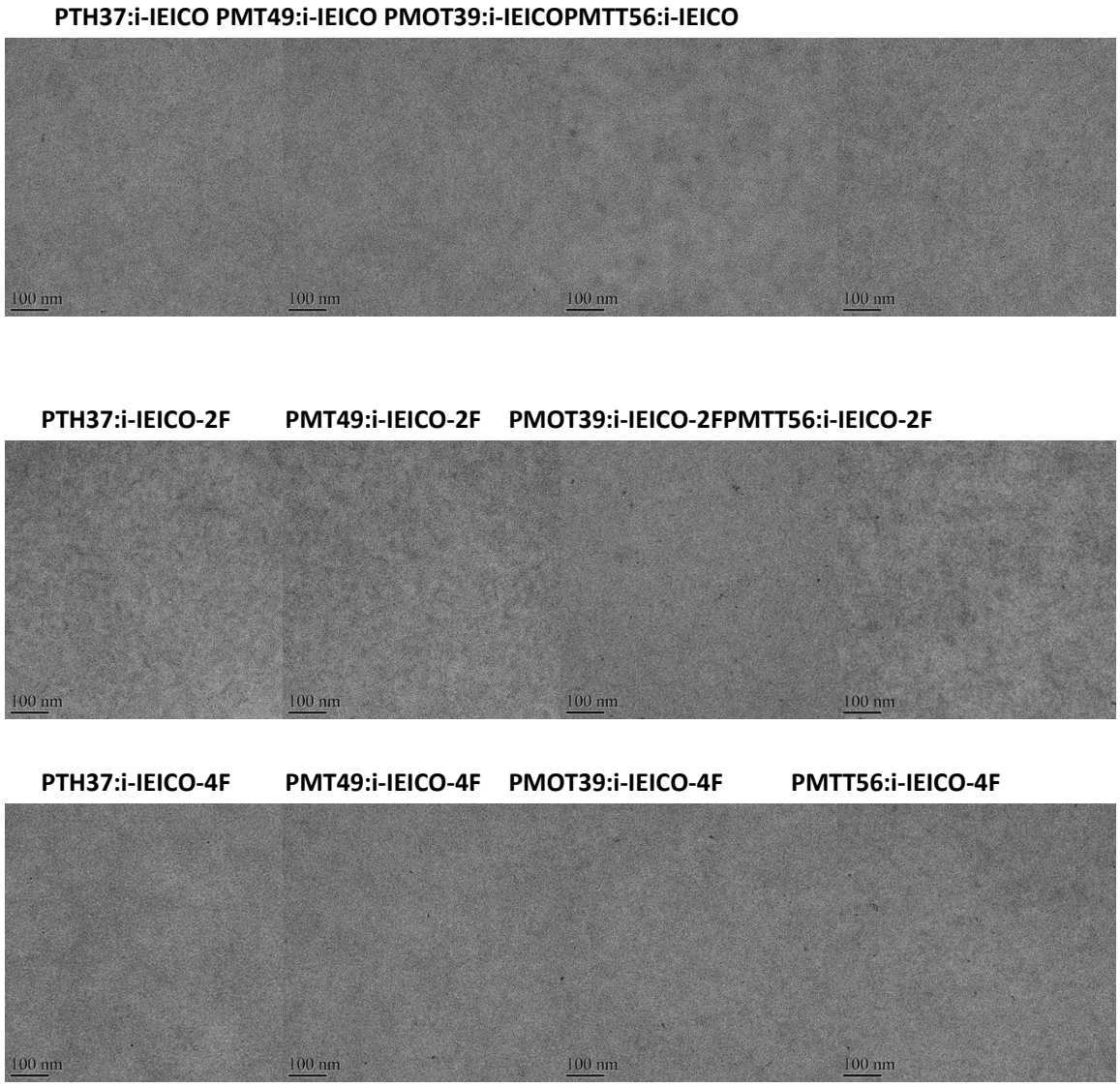

Supplementary Figure 4. Transmission electron microscope (TEM) of the blend in this study. Regardless of the overall complexity in film morphologies, the morphological difference between the blends of each group appears to be subtle. The change in aggregation for the studied blends is not significant, with 5-20 nm length scale of nanoscale phase separation that can be observed.

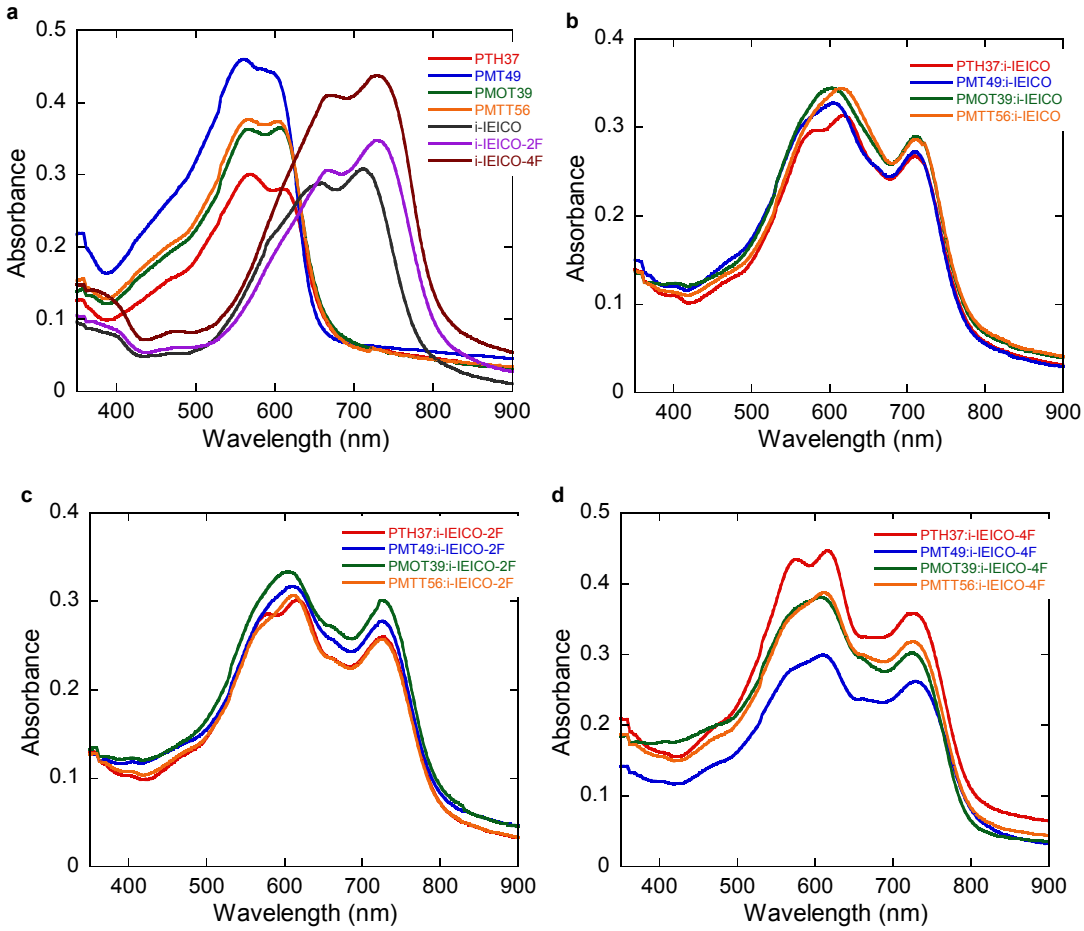

Supplementary Figure 5. Absorbance of donors, acceptors and blends. a, The absorbance of donors and acceptors neat film. **b, c, d,** the absorbance of blend films based on i-IEICO, i-IEICO-2F, i-IEICO-4F, respectively.

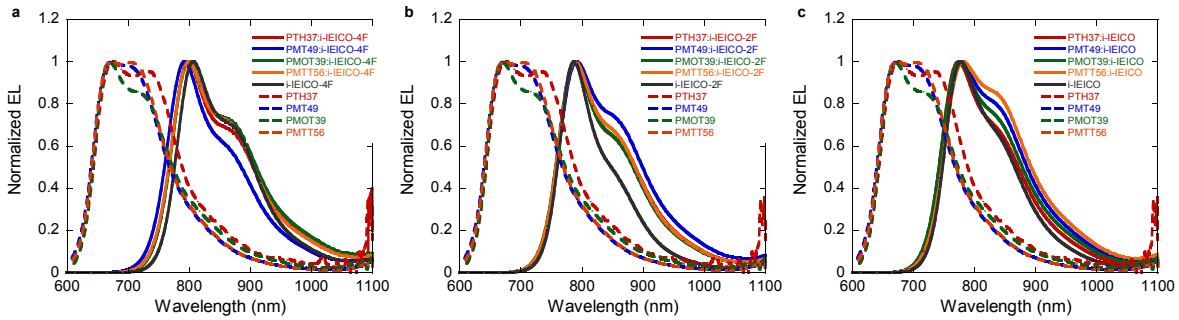

Supplementary Figure 6. Normalized electroluminescence spectra. The electroluminescence spectra of donors, acceptors and blends for i-IEICO-4F, i-IEICO-2F and i-IEICO based devices. EL of the blends is dominated by the emission of the low bandgap acceptor, while the emission from CT states is hardly detectable.

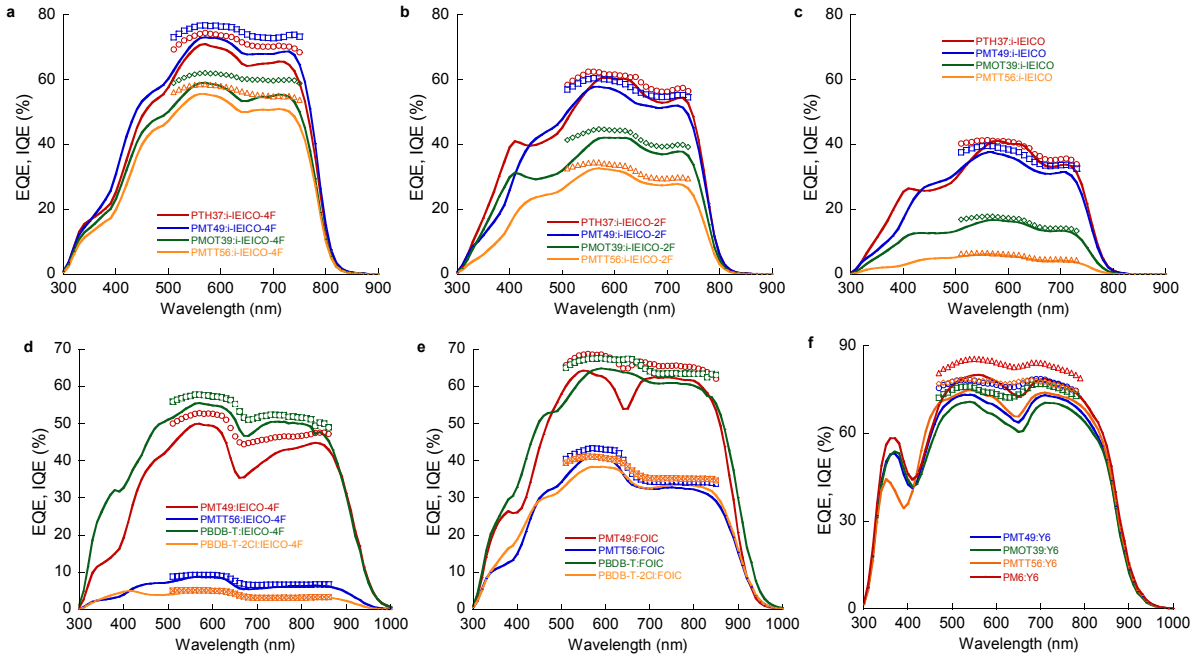

Supplementary Figure 7.EQE$_{PV}$ and IQE spectra. EQE$_{PV}$(solid lines) and IQE (symbols) spectra for devices based on different donor-acceptor blends.

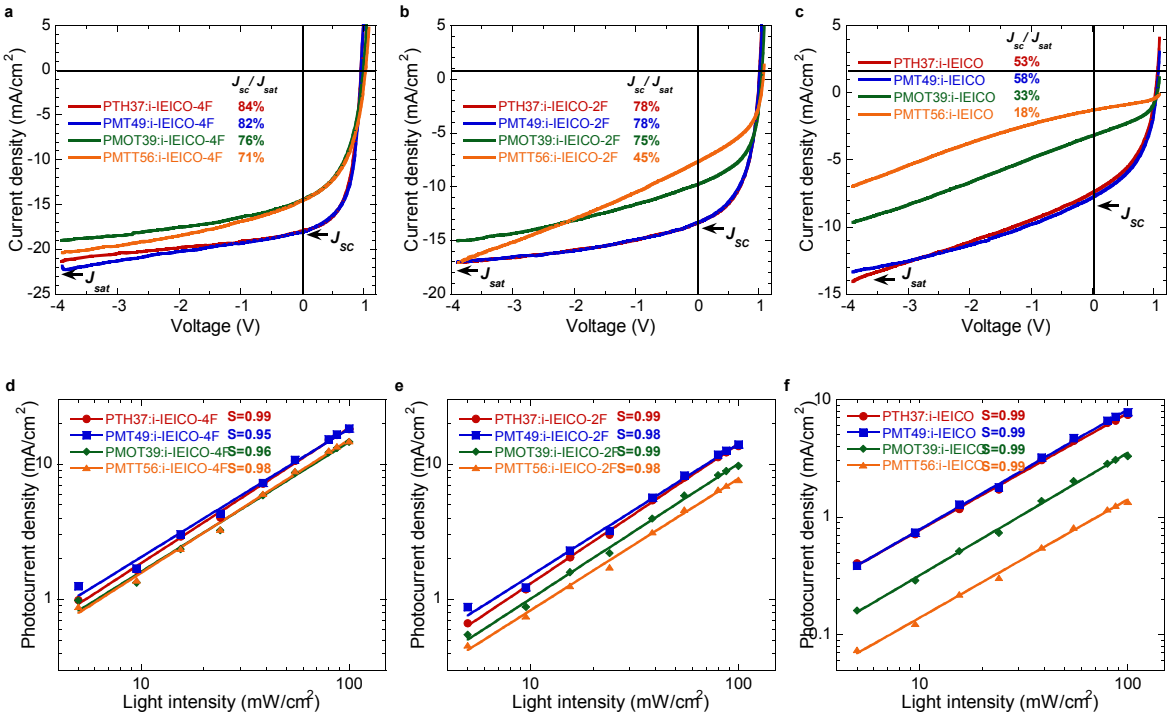

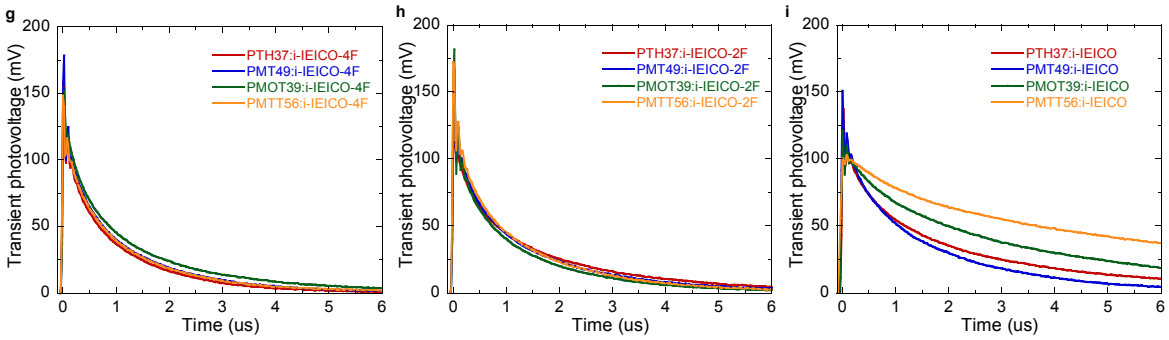

Supplementary Figure 8. Saturation current-voltage characteristics, light intensity dependent short-circuit current and transient photovoltage. a, b, c, The saturation current-voltage characteristics of i-IEICO-4F, i-IEICO-2F and i-IEICO based devices, respectively. The dissociation efficiency (J_{sat}/J_{SC}) decreases along with the energy offsets. **d, e, f,** short-circuit current density (J_{SC}) versus light intensity, J_{SC} are proportional to light intensity with slopes approaching unity, suggesting negligible non-geminate recombination for all the devices. **g, h, i,** transient photovoltage for the studied devices, the transient signals and carrier lifetimes are nearly identical for i-IEICO-4F and i-IEICO-2F based devices, indicating similar non-geminate recombination rates for these devices. The increase of carrier lifetime from PTH37 to PMT56 in i-IEICO based devices is due to a order of magnitude lower carrier density.

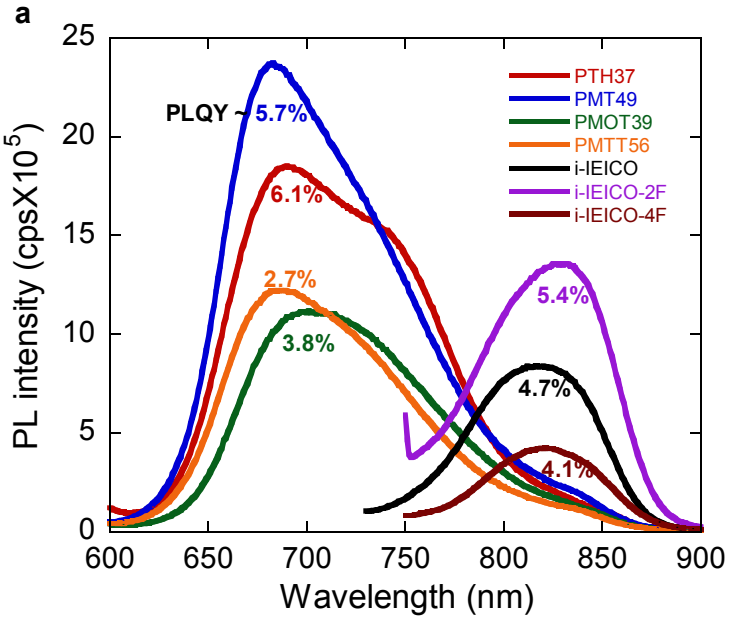

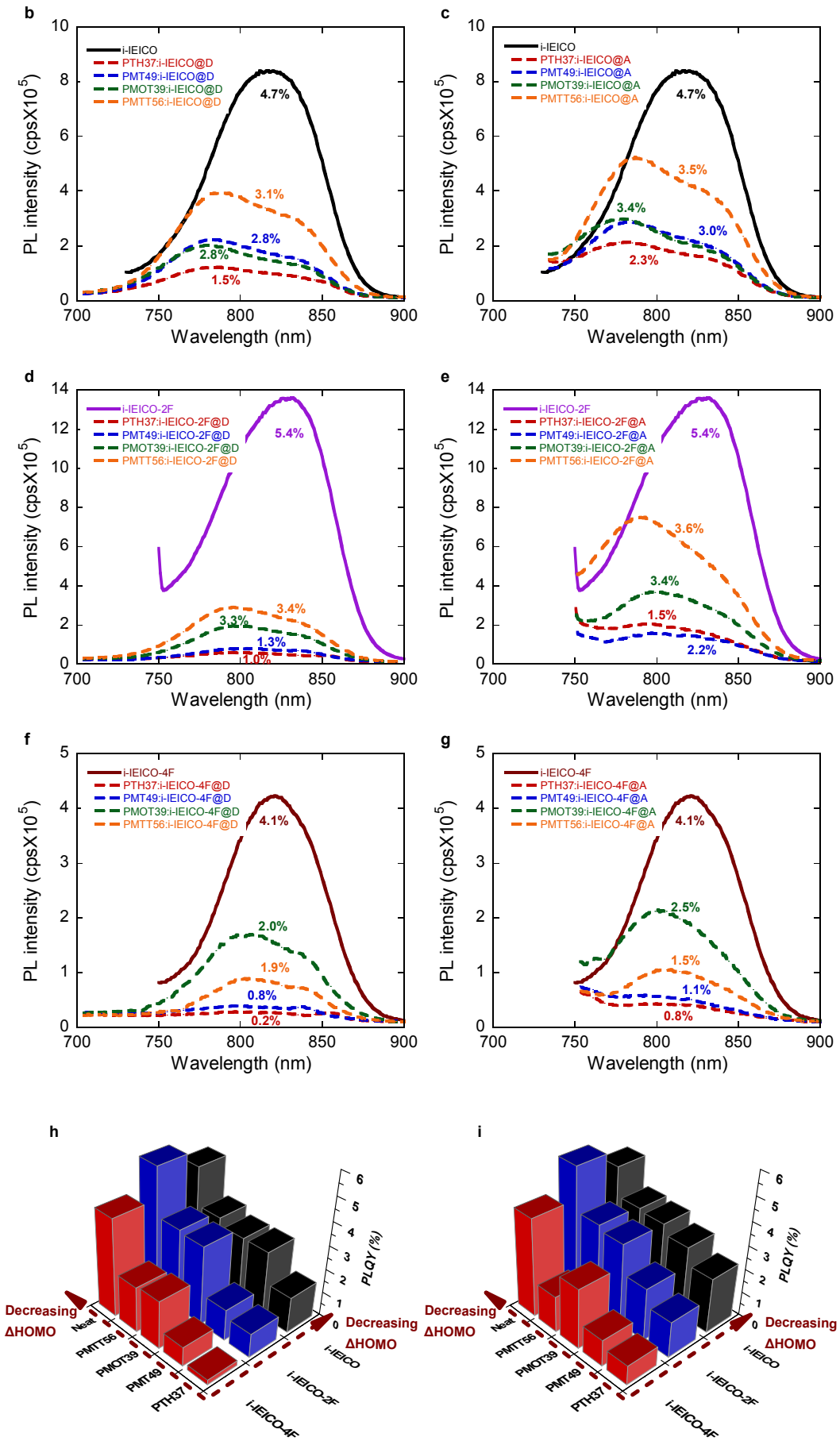
b
i-IEICO
PTH37:i-IEICO@D
PMT49:i-IEICO@D
PMOT39:i-IEICO@D
PMTT56:i-IEICO@D
4.7%
3.1%
2.8%
2.8%
1.5%
PL intensity (cpsX10^5)
Wavelength (nm)
c
i-IEICO
PTH37:i-IEICO@A
PMT49:i-IEICO@A
PMOT39:i-IEICO@A
PMTT56:i-IEICO@A
4.7%
3.5%
3.4%
3.0%
2.3%
d
i-IEICO-2F
PTH37:i-IEICO-2F@D
PMT49:i-IEICO-2F@D
PMOT39:i-IEICO-2F@D
PMTT56:i-IEICO-2F@D
5.4%
3.4%
3.3%
1.3%
1.0%
e
i-IEICO-2F
PTH37:i-IEICO-2F@A
PMT49:i-IEICO-2F@A
PMOT39:i-IEICO-2F@A
PMTT56:i-IEICO-2F@A
5.4%
3.6%
3.4%
1.5%
2.2%
f
i-IEICO-4F
PTH37:i-IEICO-4F@D
PMT49:i-IEICO-4F@D
PMOT39:i-IEICO-4F@D
PMTT56:i-IEICO-4F@D
4.1%
2.0%
1.9%
0.8%
0.2%
g
i-IEICO-4F
PTH37:i-IEICO-4F@A
PMT49:i-IEICO-4F@A
PMOT39:i-IEICO-4F@A
PMTT56:i-IEICO-4F@A
4.1%
2.5%
1.5%
1.1%
0.8%
h
i
Decreasing ΔHOMO
Neat
PMTT56
PMOT39
PMT49
PTH37
i-IEICO
i-IEICO-2F
i-IEICO-4F
PLQY (%)

Supplementary Figure 9.Photoluminescence spectra and photoluminescence quantum yield. a, The Photoluminescence spectra (PL, solid line) and absolute photoluminescence quantum yield (PLQY, labeled value) of donor and acceptor neat films obtained by two independent experiments. The donors are excited at 560nm whereas the acceptors are excited at 720 nm (see Supplementary Fig.5 for the absorptions). **b, c,** PL and PLQY of neat i-IEICO(solid line) and blends based on i-IEICO(dash line) with donor excitation (at 560 nm) or acceptor excitation (720 nm).**d, e,** PL and PLQY of neat i-IEICO-2F (solid line) and blends based on i-IEICO-2F(dash line) with donor excitation (560 nm) or acceptor excitation (720 nm). **f, g,** PL and PLQY of neat i-IEICO-4F(solid line) and blends based on i-IEICO-4F(dash line) with donor excitation (560 nm) or acceptor excitation (720 nm). **h, i,** Summary of PLQY for different systems with donor (h) or acceptor (i) excitation.

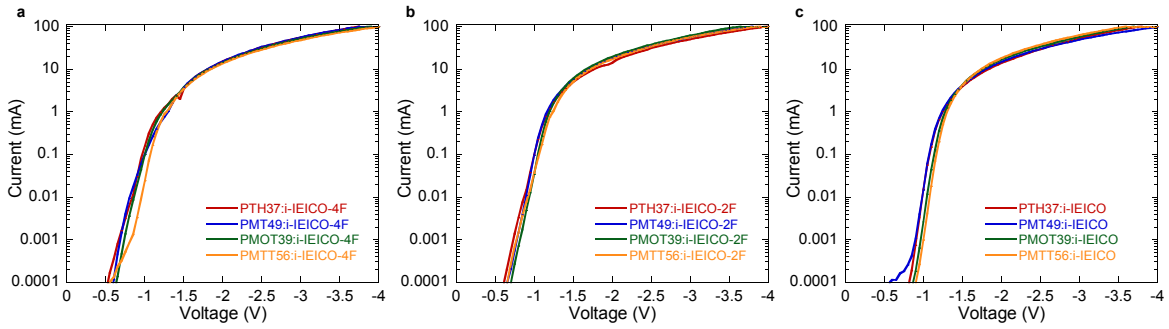

Supplementary Figure 10. Forward biased charge injection current-voltage characteristics for the studied devices. The charge injection current-voltage characteristics remain unchanged while replacing the donor for each acceptor, suggesting that the charge injection from anode to the donors remain unhindered while changing the HOMO level of donor. The negative signs in voltage is due to the inverted structure of the devices.

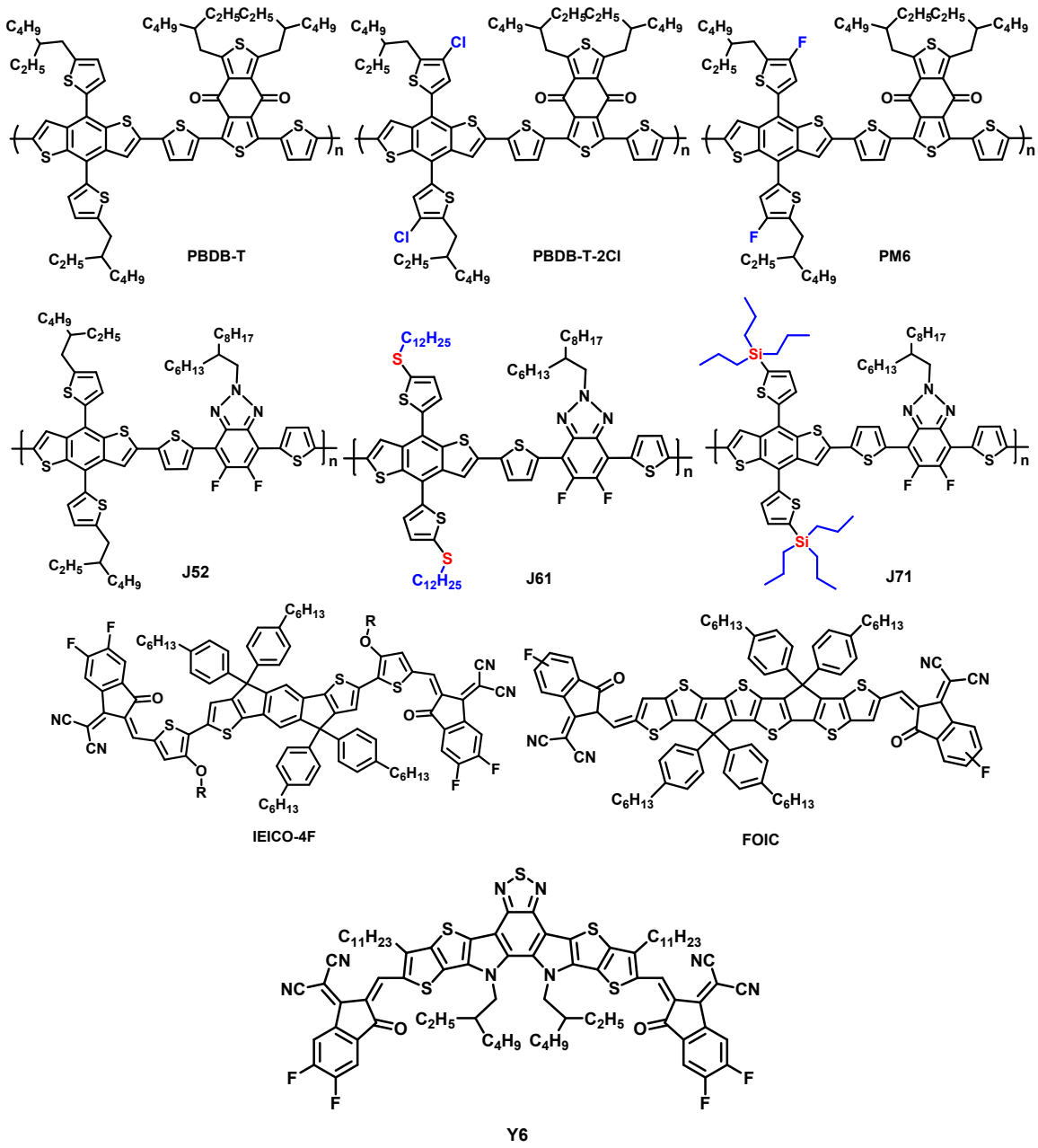

Supplementary Figure 11. Molecular structures of literature compounds used in this study. The chemical modifications to enable energy level differences for each donor series are highlighted in blue.

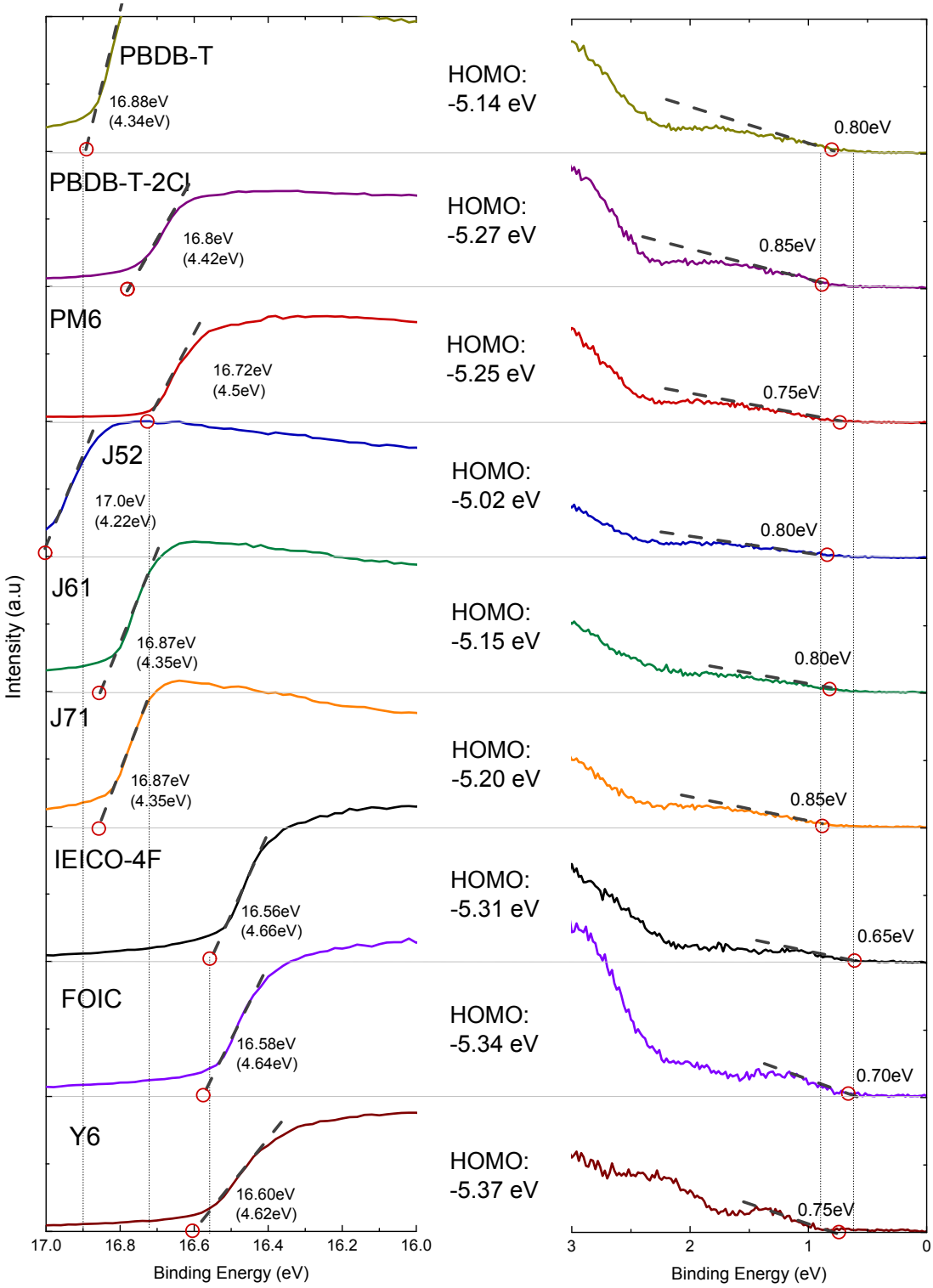

Supplementary Figure 12. Ultraviolet Photoelectron Spectroscopy (UPS) spectra of materials studied. High binding energy cutoff (left) and HOMO region (right) of UPS spectra are shown for donors and acceptors. The spectra width is defined by energy difference between two regions, in which liner fit of slope intersects (grey dash line) with baseline gives the binding energy. The HOMO levels (middle) are calculated by subtracting the spectra

width from the He I excitation energy (21.22 eV).

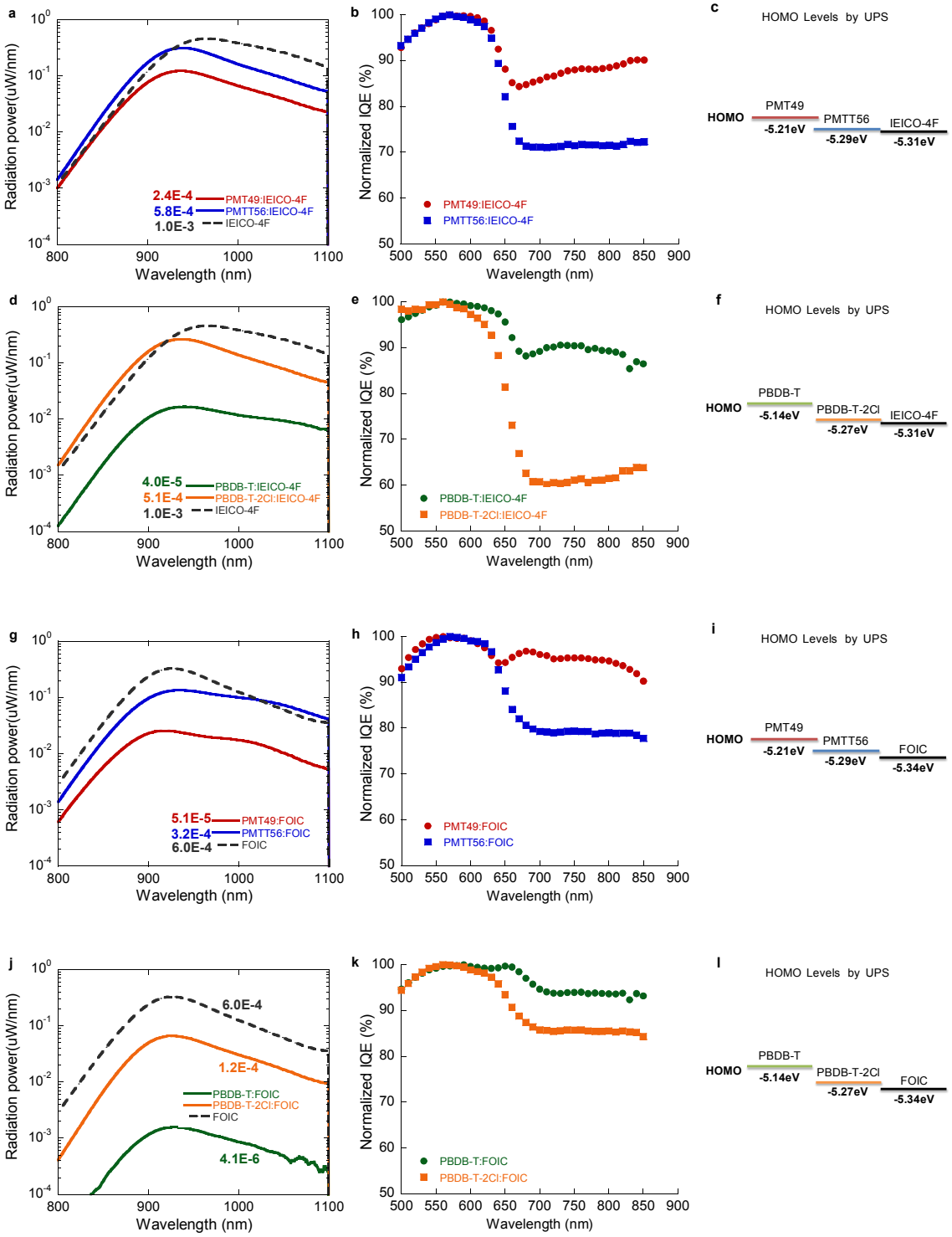

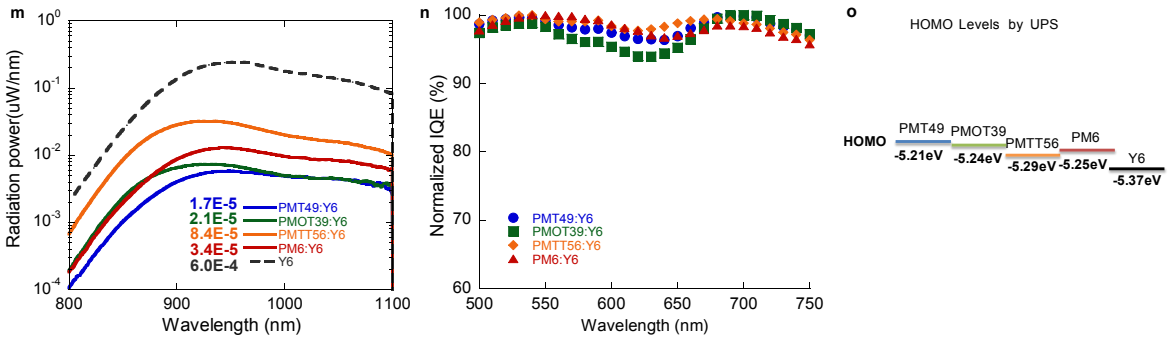

Supplementary Figure 13.EL intensity, normalized IQE and HOMO level diagram in IEICO-4F, FOIC and Y6 blends. a, b, c, d, e, f, EL intensity, normalized IQE and HOMO level diagram for IEICO-4F based devices. **g, h, i, j, k, l,** EL intensity, normalized IQE and HOMO level diagram IQE for FOIC based devices. **m, n, o,** EL intensity, normalized IQE and HOMO level diagram for Y6 based devices. Calculated EQE_{EL} is labeled with the same color. The grey dash line denotes the EL intensity of neat acceptor device, all the devices are forward biased with constant injecting current during EL experiment. All systems show enhanced EL intensity toward acceptor with the EL intensity of neat acceptor (grey dash line) as an upper limit, and reduced PHT efficiency when HOMO offset decreases.

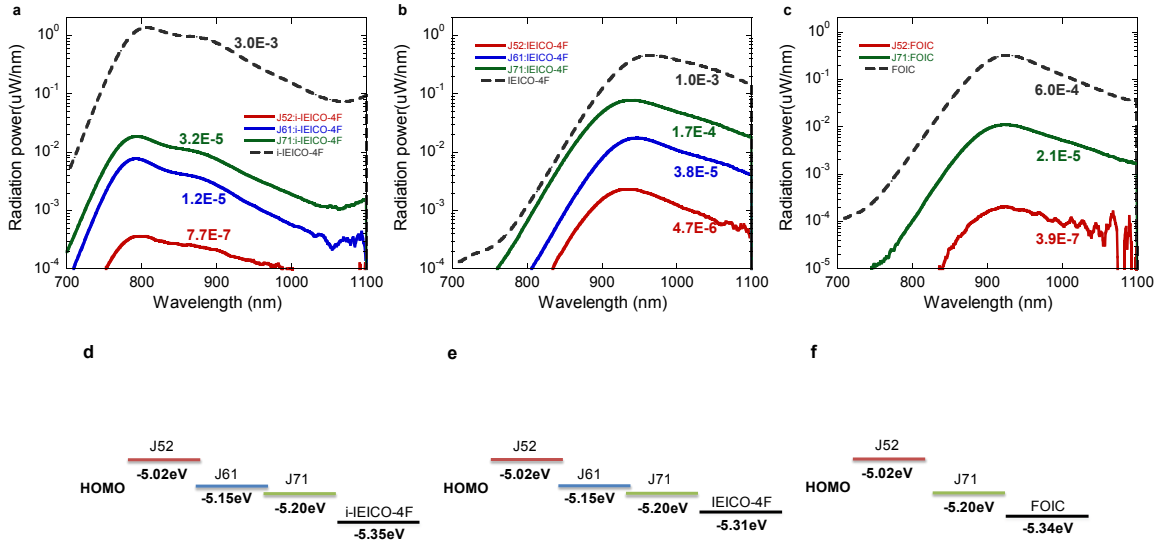

Supplementary Figure 14.EL intensity and HOMO level diagram for device with J51, J61, J71. The EL intensity and HOMO level diagram of polymer donor J51, J61, J71blend with **a,** i-IEICO-4F, **b,** IEICO-4F and **c,** FOIC. Measured EQE_{EL} is labeled with the same color. The devices are forward biased with constant injecting current. The EL intensity of blend increases when decreasing HOMO offset, with the EL intensity of neat acceptor (grey dash line) as an upper limit.

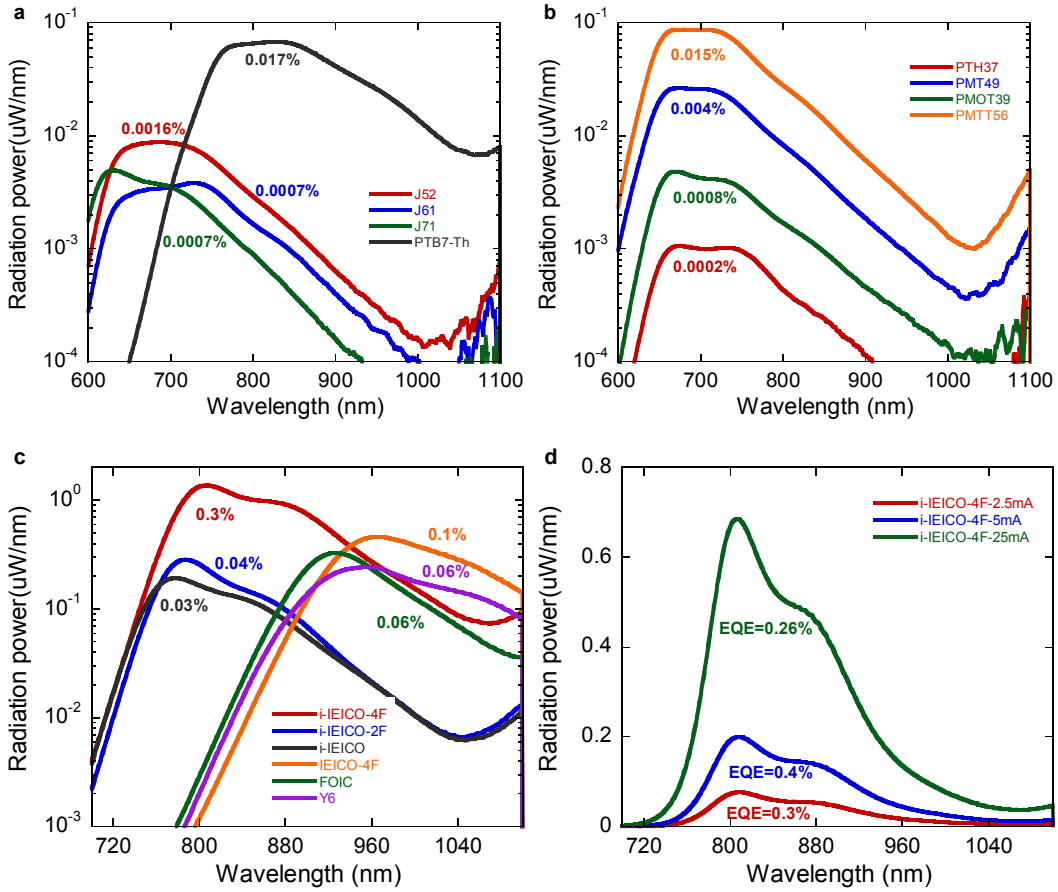

Supplementary Figure 15. EL intensity and EQE_{EL} of donor and acceptor neat films. a, EL intensity of J52, J61, J71 and PTB7-Th neat films when forward biased with constant injecting current. The percentage with same color labels the calculated EQE_{EL}. **b,** The EL intensity and EQE_{EL} of PTH37, PMT49, PMOT39 and PMTT56 when forward biased with constant injecting current. **c,** The EL intensity and EQE_{EL} of i-IEICO-4F, i-IEICO-2F, i-IEICO, IEICO-4F, FOIC and Y6 when forward biased with constant injecting current. **d,** The EL intensity and EQE_{EL} of i-IEICO-4F with different injecting current.

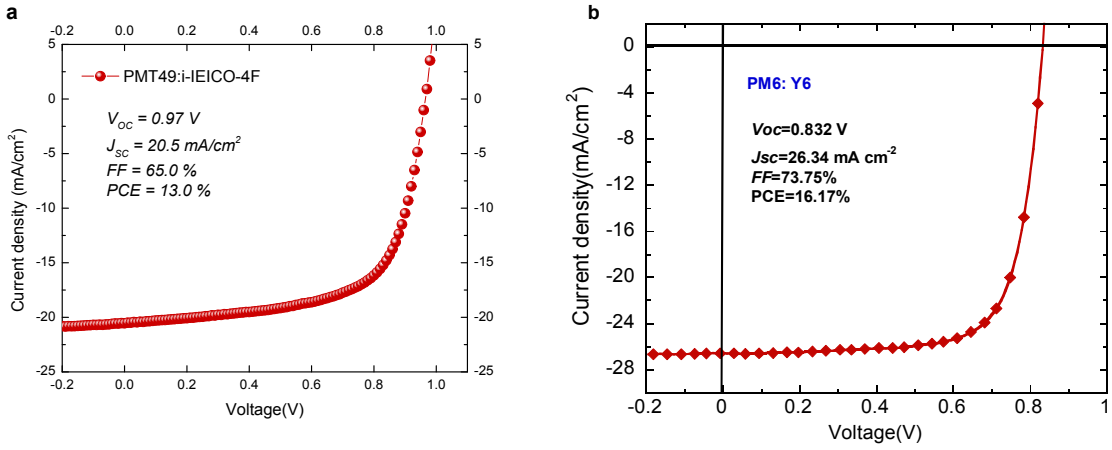

Supplementary Figure 16. J-V characteristic of PMT49:i-IEICO-4F (a) and PM6: Y6 (b). J-V characteristic of PMT49:i-IEICO-4Fdevice and **PM6: Y6 device** under 1 sun, AM 1.5G illumination, respectively.

Table S1Photovoltaic parameters and radiative efficiency for blends in this study. The data shown in brackets are the average values and standard deviations, which are evaluated from over eight independent devices. The optical bandgaps (E_g) is defined as the energy of half EQE_{PV} maximum from low bandgap acceptors($E_{g,half}$), aside from PDPP3T blends. The radiative efficiencies (EQE_{EL}) are obtained by electroluminescence experiment, and the non-radiative voltage losses are calculated by equation1 in the main text.

Active layer	E_g/q (V)	V_{OC} (V)	Jsc (mA/cm^2)	FF (%)	PCE (%)	E_g/q-V_{OC} (V)	EQE_{EL}	$\Delta V_{OC}^{non\text{-}rad}$ (V)
PTB7-Th:i-IEICO-4F	1.57	0.83 (0.822±0.008)	16.5 (16.8±0.4)	56.3 (54.1±2.6)	7.76 (7.44±0.29)	0.74	3.1×10^{-6}	0.33
J52:i-IEICO-4F	1.57	0.87 (0.863±0.006)	19.5 (19.1±0.3)	60 (61.1±1.4)	10.18 (10.09±0.15)	0.7	7.7×10^{-7}	0.37
J61:i-IEICO-4F	1.57	0.94 (0.940±0.000)	17.6 (17.2±0.3)	56.8 (57.7±0.7)	9.4 (9.30±0.09)	0.63	1.2×10^{-5}	0.29
J71:i-IEICO-4F	1.57	0.97 (0.963±0.006)	16.6 (17.2±0.6)	54.1 (52.8±1.2)	8.72 (8.76±0.06)	0.6	3.2×10^{-5}	0.27
PTB7-Th:IEICO-4F	1.35	0.72 (0.720±0.000)	22.9 (23.2±0.2)	56.2 (55.3±0.7)	9.27 (9.25±0.04)	0.63	8.3×10^{-6}	0.30
J52:IEICO-4F	1.35	0.73	21.8	48.4	7.72	0.62	4.7×10^{-6}	0.32

		(0.718±0.004)	(20.3±0.4)	(50.8±0.5)	(7.40±0.11)			
J61:IEICO-4F	1.35	0.75 (0.746±0.005)	16.2 (16.3±0.3)	48.9 (47.3±1.8)	5.94 (5.84±0.15)	0.6	3.8×10^{-5}	0.26
J71:IEICO-4F	1.35	0.82 (0.811±0.004)	12.9 (12.6±0.4)	34 (34.1±0.5)	3.61 (3.48±0.15)	0.53	1.7×10^{-4}	0.23
PBDB-T:IEICO-4F	1.35	0.78 (0.765±0.010)	16.3 (15.6±0.6)	36.8 (35.5±1.2)	4.71 (4.24±0.33)	0.57	4.0×10^{-5}	0.26
PBDB-T-2Cl:IEICO-4F	1.35	0.86 (0.83±0.029)	1.52 (1.49±0.4)	32 (31.2±2.3)	0.42 (0.39±0.37)	0.49	5.1×10^{-4}	0.20
PMT49:IEICO-4F	1.35	0.85 (0.849±0.004)	12.5 (12.4±0.1)	42.2 (41.9±0.5)	4.5 (4.41±0.09)	0.5	2.4×10^{-4}	0.22
PMTT56:IEICO-4F	1.35	0.87 (0.865±0.007)	3.5 (3.3±0.4)	31.3 (32.1±1.0)	0.99 (0.91±0.11)	0.48	5.8×10^{-4}	0.19
PTB7-Th:FOIC	1.40	0.69 (0.690±0.000)	22.4 (22.3±0.3)	65.7 (65.1±1.0)	10.16 (10.00±0.20)	0.71	2.9×10^{-6}	0.33
J52:FOIC	1.40	0.66 (0.662±0.004)	24.9 (25.4±0.5)	51.9 (49.8±1.4)	8.53 (8.36±0.18)	0.74	3.9×10^{-7}	0.38
J71:FOIC	1.40	0.77 (0.755±0.013)	20.3 (20.3±0.6)	54 (53.4±0.8)	8.48 (8.19±0.29)	0.63	2.1×10^{-5}	0.28
PBDB-T:FOIC	1.40	0.69 (0.686±0.005)	21.2 (20.8±0.4)	44.4 (43.2±1.2)	6.53 (6.19±0.29)	0.71	4.1×10^{-6}	0.32
PBDB-T-2Cl:FOIC	1.40	0.83 (0.828±0.004)	12.7 (12.8±0.3)	54.3 (52.2±1.8)	5.75 (5.51±0.13)	0.57	1.2×10^{-4}	0.23
PMT49:FOIC	1.40	0.82 (0.816±0.005)	20.7 (20.8±0.1)	53.6 (52.6±1.6)	9.11 (8.91±0.24)	0.58	5.1×10^{-5}	0.26
PMTT56:FOIC	1.40	0.87 (0.870±0.006)	14.3 (12.8±0.5)	56.8 (55.7±1.5)	7.08 (6.18±0.32)	0.53	3.2×10^{-4}	0.21
PTB7-Th:ITIC	1.65	0.78 (0.803±0.005)	15.8 (16.1±0.7)	61.2 (58.6±1.8)	7.54 (7.58±0.16)	0.87	1.0×10^{-6}	0.36
PDPP3T:IDIC	1.36	0.71 (0.714±0.005)	10.5 (10.4±0.2)	62.7 (61.1±1.7)	4.68 (4.56±0.17)	0.65	3.4×10^{-6}	0.33
PDPP3T:ITIC-Th	1.36	0.74 (0.742±0.008)	5.66 (5.6±0.1)	54.5 (54.1±0.7)	2.28 (2.25±0.02)	0.62	8.8×10^{-6}	0.30
PDPP3T:ITIC	1.36	0.77 (0.770±0.000)	3.74 (3.6±0.1)	53.7 (52.8±0.8)	1.54 (1.46±0.05)	0.59	2.1×10^{-5}	0.28
PDPP3T:IT-M	1.36	0.76 (0.757±0.006)	2.04 (2.0±0.1)	47.3 (46.9±1.5)	0.73 (0.72±0.01)	0.60	1.6×10^{-5}	0.29
PMT49:Y6	1.43	0.81 (0.804±0.005)	26 (25.4±0.5)	51.2 (50.3±1.3)	10.81 (10.26±0.47)	0.63	1.7×10^{-5}	0.29
PMOT39:Y6	1.43	0.82 (0.818±0.004)	22.1 (21.8±0.7)	49.3 (47.5±1.3)	8.97 (8.48±0.44)	0.62	2.1×10^{-5}	0.28
PMTT56:Y6	1.43	0.86 (0.861±0.004)	26.4 (26.0±0.6)	50.9 (49.4±1.3)	11.59 (11.07±0.38)	0.58	8.4×10^{-5}	0.24
PM6: Y6	1.43	0.83	26.3	73.8	16.17	0.59	3.4×10^{-5}	0.27

(0.835±0.004) (26.9±0.8) (72.7±1.5) (16.32±0.22)

References

1. M. L. Tietze, W. Tress, S. Pfützner, C. Schünemann, L. Burtone, M. Riede, K. Leo, K. Vandewal, S. Olthof, P. Schulz and A. Kahn, *Phys. Rev. B*, 2013, **88,** 085119.
2. Y. Wang, D. Qian, Y. Cui, H. Zhang, J. Hou, K. Vandewal, T. Kirchartz and F. Gao, *Adv. Energy Mater.*, 2018, **8**, 1801352.
3. V. C. Nikolis, J. Benduhn, F. Holzmueller, F. Piersimoni, M. Lau, O. Zeika, D. Neher, C. Koerner, D. Spoltore and K. Vandewal,*Adv. Energy Mater.*, 2017, **7**, 1700855.
4. K. Vandewal, J. Benduhn and V. C. Nikolis, *Sustainable Energy & Fuels*, 2018, **2**, 538-544.
5. U. Rau, B. Blank, T. C. M. Müller and T. Kirchartz, *Phys. Rev. Appl.*, 2017, **7**, 044016.